Electrolyte and temperature effects in a rising bubble

Mandalahalli, Manas M.; Lif, Johan; Mudde, Robert F.; Portela, Luis M.

DOI
10.1016/j.ces.2022.118276

Publication date
2023

Document Version
Final published version

Published in
Chemical Engineering Science

Chemical Engineering Science 270 (2023) 118276

Contents lists available at ScienceDirect

Chemical Engineering Science

journal homepage: www.elsevier.com/locate/ces

Electrolyte and temperature effects in a rising bubble

Manas M. Mandalahalli [a], Johan Lif [b], Robert F. Mudde [a], Luis M. Portela [a,*]

[a] Transport Phenomena Group, Department of Chemical Engineering, Delft University of Technology, Van der Maasweg 9, 2629HZ Delft, the Netherlands
[b] Nouryon Pulp and Performance Chemicals, Färjevägen 1, 44534 Bohus, Sweden

HIGHLIGHTS

- Single H_2 bubble rise in water and (mixture)-electrolytes at different temperatures.
- Bubble rise characteristics show a pure-liquid behaviour, dependent only on ρ, μ, σ.
- Non-dimensional parameter $ReWe^{-2/3}Mo^{1/5}$ is constant within a flow regime.

ARTICLE INFO

Article history:
Received 9 February 2021
Received in revised form 20 October 2022
Accepted 2 November 2022
Available online 8 November 2022

Keywords:
Bubble rise
Electrolytes
Non-dimensional analysis
Temperature effect

ABSTRACT

In this work, the rise characteristics of a single H_2 bubble, in the ellipsoidal regime, in (i) water, (ii) single electrolyte (2 M, 4.5 M NaCl) solution and (iii) various concentrations of electrolyte mixture (up to 6.4 M of 1:5 weight fraction NaCl-$NaClO_3$), have been studied, at temperatures up to 80°C. Our results show that both individual and collective effects of the temperature and the electrolyte concentration on the rise velocity and the bubble shape are purely dependent on the changes in liquid properties (density, viscosity, and surface tension); the bubble motion can be described by known non-dimensional correlations for clean bubble rise in pure fluids.

1. Introduction

Gas–liquid unit operations are widely used in many (bio)-chemical processes, such as electrolysis, wastewater treatment, froth-flotation, and Fischer–tropsch synthesis (e.g. Liu et al., 2013; Jean and Lee, 1999). An essential aspect of the design and scale-up of the gas–liquid contacting equipment, such as bubble and airlift columns, is a phenomenological understanding of the interactions between the two phases. Changes in process conditions (temperature, pressure, pH, etc.) or the presence of dissolved substances (salts, surfactants, etc.) can have a strong influence on the hydrodynamic parameters (gas holdup, bubble size distribution, rise velocities) and, thereby, influence the performance of these processes. While many industrial processes are operated at non-ideal conditions of high pressure/temperature in presence of contaminants (Rollbusch et al., 2015), current design models are mostly based on well-known bubble rise characteristics in pure fluids at ambient conditions. It is therefore of interest to better understand the micro-phenomena at industrially-relevant conditions, even for a single bubble. In the current work, we focus on the effects of the liquid temperature and dissolved electrolytes at high concentrations on the rise characteristics of a single ellipsoidal bubble.

The rise characteristics of a single bubble have been extensively studied, analytically, numerically and experimentally (e.g. Kulkarni and Joshi, 2005; Moore, 1959; Loth, 2008; Tripathi et al., 2015). A fundamental understanding of the bubble shape and (terminal) rise velocity is based on the interplay between the different forces involved and the flow around the bubble, as schematized in Fig. 1a. Buoyancy, the driving force, is a volume force, dependent on the volume of the bubble (expressed through the equivalent bubble diameter, d_{eq}) and the difference in gas and liquid densities, $\Delta\rho$ (= density of liquid, ρ, considering a relatively negligible density of the gas phase). Once a terminal situation is reached, the buoyancy force (on average) is balanced by the drag force.

For a spherical bubble rising with a free-slip interfacial condition (a clean bubble), the interfacial tangential force, F_{int}, is equal to zero, and, as a result, there does not exist any wake separation at all Reynolds numbers ($Re=\rho U_b d_{eq}/\mu$). In this case, the non-dimensional drag force expressed through the drag coefficient, C_D, depends only on the Reynolds number, i.e. $C_D = f(Re)$, with $C_D = 16/Re$ in the limit of very low Re ($Re \to 0$) and $C_D =$

* Corresponding author.
E-mail addresses: m.m.mandalahalli@tudelft.nl (M.M. Mandalahalli), l.portela@-tudelft.nl (L.M. Portela).

https://doi.org/10.1016/j.ces.2022.118276
0009-2509/

Nomenclature

Latin

Re	Reynolds number [-]
Eo	Eötvös number [-]
Mo	Morton number [-]
We	Weber number [-]
C_D	Drag Coefficient [-]
F_B	Bouyancy force[N]
F_σ	Surface tension force [N]
U_b	Bubble rise velocity [m/s]
U_T	Terminal rise velocity [m/s]
T	Liquid temperature [°C]
d_{eq}	Equivalent bubble diamter [mm]
d_N	Nozzle inner diameter [mm]

Greek

σ	Surface tension [mN/m]
ρ	Liquid density [kg/m^3]
μ	Liquid viscosity [Pa.s]
χ	Bubble aspect ratio [-]
μ	Liquid viscosity [Pa.s]

Subscripts

emp	Empirical
expt	Experimental

$48/Re$ in the limit of very high Re ($Re \to \infty$) (Levich, 1949; Moore, 1963; Kang and Leal, 1988; Mei et al., 1994; Sun and Klaseboer, 2022). Small bubbles at low Re are spherical, however, for larger and deformable bubbles ($Re \gtrapprox 10^2$), surface tension (σ) plays a strong role in dictating the shape and, thereby, the drag force acting on the bubble. Therefore, C_D for larger deformable bubbles will differ from the high Re limit of $C_D = 48/Re$ for spherical bubbles.

In the case of clean bubbles in pure fluids, such as deminarilized water, the bubble rise characteristics can be expressed in terms of three independent non-dimensional numbers, which, collectively, include the gravity (g), the liquid properties (density ρ, viscosity μ, and surface tension σ), the bubble rise velocity (U_b) and the bubble size (d_{eq}). Most commonly used non-dimensional numbers are: Reynolds ($Re=\rho U_b d_{eq}/\mu$), Eötvös ($Eo=\rho g d_{eq}^2/\sigma$), Morton ($Mo=\mu^4 g/\rho\sigma^3$) and Weber ($We=\rho U_b^2 d_{eq}/\sigma$). This is well-known from the *classical* empirical regime map from Clift et al. (1978) and non-dimensional correlations (e.g. Loth, 2008).

The interfacial rheology, i.e. the relation between the interfacial stresses (F_{int} in Fig. 1a) and the interfacial (rate of) deformation (e.g. Edwards et al., 1991) can have a strong effect on the interplay between the different forces involved and the flow around the bubble, and, therefore, on the rise characteristics of the bubble. For example, a nofree shear interface (schematized in Fig. 1b) can affect the wake separation. The interfacial rheology is characterized through extra properties, like interfacial viscosity and elasticity. Therefore, if it plays a significant role, this would lead to the appearance of extra non-dimensional numbers associated with these properties, and the bubble rise characteristics could no longer be expressed in terms of only three independent non-dimensional numbers.

Interfacial rheological effects can be due to contaminants (e.g. surface active molecules or ions) at the interface and depend on the nature of the contaminant (salt, surfactant, etc.) and its concentration. A well-studied example is the case of a bubble rise in tap water, where a higher resistance to the bubble motion and a reduction in rise velocity is attributed to additional tangential stress caused by a non-uniform surface concentration, as adsorbed trace molecules at the interface are advected to the rear of the bubble (Fdhila and Duineveld, 1996); contrary to a pure liquid, $F_{int} \neq 0$ in this case. In certain cases, instead of a free-slip condition one could have a no-slip interfacial condition. Bubble size and genera-

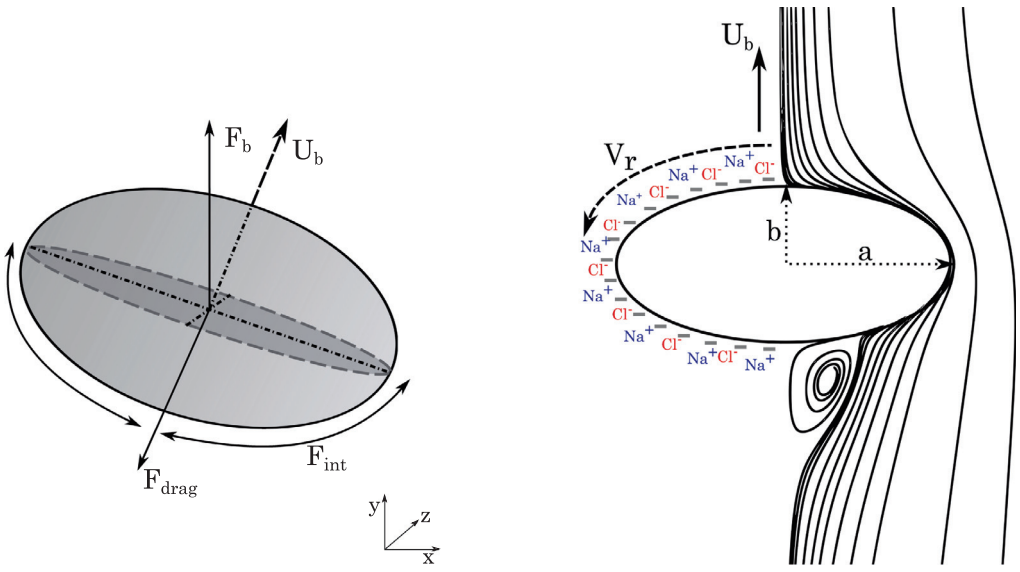

(a) (b)

Fig. 1. Schematic of an ellipsoidal rising bubble, with a velocity (U_r). Panel (a): forces acting on a rising bubble (F_b: buoyancy force; F_{drag}: drag force; F_{int}: interfacial tangential force). Panel (b): Axisymmetric flow around an ellipsoidal bubble in an electrolyte (NaCl) solution; the relative velocity at the interface (V_r) is strongly dependent on the interfacial rheology, therefore, it could depend on the concentration and ionic properties of Na^+ and Cl^-.

tion method also influence the contaminant effect on the bubble motion; the slower the bubble generation, the higher the surfactant concentration at the interface (Peters and Els, 2012).

In the case of dissolved electrolytes, ions usually are repelled from the gas–liquid interface. Resulting electrostatic repulsions and ionic mobility lead to an increase in interfacial tension. Ion interactions at the interface are further explained in detail in Appendix B. At low concentrations (0.1–1.0 M (moles/liter)), due to a marginal increase in surface tension, electrolytes can be considered as a weak contaminant. However, earlier investigations (Kracht and Finch, 2010; Quinn et al., 2014) observed that low concentrations ($\mathcal{O}$(0.1 M)) are sufficient to cause a strong reduction in the rise velocity for ellipsoidal bubbles ($d_{eq} \sim 2$ mm). On the contrary, recently, Hessenkemper et al. (2020) showed only a marginal decrease and noted that higher concentrations would be required to significantly affect the rise velocity. While existing investigations differ in their conclusions, the studies are limited to a maximum concentration of 1 M (mol/liter); there are no significant changes to the liquid properties in this range. At higher concentrations, a large presence of ions close to the interface could influence the interfacial rheology. Meanwhile, an increase in all three liquid properties (ρ, μ, σ) can also play a significant role in the rise characteristics, from a clean bubble in a pure liquid perspective.

An increase in the liquid temperature from ambient conditions has a strong influence on the properties of the liquid. Whereas a lower liquid density reduces the buoyancy force, a decrease in both viscosity and surface tension can affect the drag force experienced by the bubble. There are only limited studies in the literature for the case where the gas bubble and the liquid are in thermal equilibrium (Kulkarni and Joshi, 2005). For temperature up to 45 °C, Zhang et al. (2003) and Leifer et al. (2000), respectively, observed a non-effect and a increase in the rise velocity with an increase in the temperature. Studying bubble rise at two temperatures: 10 °C and 90 °C, Okawa et al. (2003) showed a decrease in the rise velocity at the higher temperature. While the available literature studies are performed in deminarlized water, the available experimental data do not provide a consistent conclusion on the effect of temperature and do not agree with the predictions for pure fluids (from Clift et al. (1978)). A systematic understanding of the temperature effect on the rise characteristics is, therefore, required.

In the current work, we study the effects of liquid temperature (up to 80 °C) and strong (mixture) electrolytes (up to saturated concentrations of sodium chlorate-chloride mixtures in water), both individually and collectively, on the bubble shape and rise velocity. The main purpose is to determine whether a change in the rise characteristics under the conditions of high temperature and high electrolyte concentration can be explained by currently-known clean bubble pure-fluid correlations based entirely on the changes in the corresponding liquid properties.

2. Experimental methodology

2.1. Fluids used: physical properties

The gas–liquid system used in the current experiments is relevant for industrial Chlor-alkali and Chlorate electrolysis processes. Electrolytes used are sodium chloride (NaCl, ACS analytical grade, $\geqslant$99.5% pure) and sodium chlorate ($NaClO_3$, industrial grade, $\geqslant$99.6% pure). Hydrogen gas is used as the gas phase. Demineralized water, solution of sodium chloride in water (2 M, 4.5 M), and four concentrations of sodium chloride-chlorate mixture (1:5 weight fraction of NaCl:$NaClO_3$) in water are used as liquids. The four mixture concentrations correspond to 1.28 M (20% mix.), 2.56 M (40% mix.), 3.85 M (60% mix.), and 6.4 M (100% mix.) in ionic strength. The 100% mixture is prepared by mixing 100 g/L and 500 g/L of NaCl and $NaClO_3$ respectively; it is diluted to obtain 20%, 40% and 60% mixtures. Experiments are performed at four temperatures: 25, 40, 60, and 80 °C. The mixture concentration is chosen to avoid precipitation of the salts at all temperatures. Liquid properties (density, viscosity, and surface tension) for all liquids used in the current experiments are listed in Table A.1. The density data is determined from weight measurements of each fluid in a 100 ml standard bottle at several temperatures. The viscosity measurements at several temperatures are done using a Ostwald viscometer. The density and viscosity data (in Table A.1) is based on a correlation derived from a series of measurements at different temperatures, with a typical accuracy of 2 kg/m^3 and 0.05x10^{-3} Pa.s, respectively. The surface tension of the fluids is measured using the axisymmetric drop shape analysis method (ADSA) (Saad and Neumann, 2016). The ADSA measurement technique and the results obtained are explained in Appendix C.

2.2. Experimental setup

The experimental apparatus is shown in Fig. 2. The experiments are carried out in a jacketed cylindrical column 0.750 m x 0.15 m (height x diameter). The temperature in the column is controlled using hot water flow through the jacketed part, connected to a thermostatic water bath. Temperature, measured using a wire probe, shows a maximum deviation of 0.4 °C throughout the column. The hydrogen bubble in the column is generated through a single submerged needle of internal diameter 0.13 mm. Flow through the needle is controlled using precision dosing meters (MetroOhm Dosimat 876). The submerged gas inlet tubing ensures that the generated bubble and the liquid are at the same temperature. In order to generate bubbles at a low frequency, ensuring a slow growth of the bubble at the needle, the flow rate is set at a low 0.1 ml/min ($\approx$ 1 bubble every 2.5 s). Electrolyte solutions are prepared separately and added to the column. For electrolyte corrosion resistance, both the needle and the needle holder are made out of titanium. Hydrogen, compared to dissolving CO_2 gas, has a low solubility in both water and brine (Cygan, 1991; Haynes, 2009); any dissolution effect during the bubble rise can be ignored. A continuous flow of hydrogen bubbles can create an explosive mixture with ambient air at the top surface of the liquid, with a flammable limit of 4% H_2 in air (v/v) (Haynes, 2009). To avoid this, the liquid surface is purged with a continuous flow of N_2 gas.

Images of a single bubble released from the needle are acquired using two high-speed USB cameras (Basler Aca-1920-150uc, max. resolution 1920x1200 px^2) at a rate of 200 frames/s. Camera 1, as shown in the schematic (Fig. 2), is used to measure the growth of the bubble, with a pixel resolution of 75.8 pixel/mm. This camera is further raised to capture images at mid-column height, in order to measure the bubble shapes at terminal conditions. Camera 2, with a resolution of 17.5 pixel/mm, is used to acquire the bubble motion through the column, for trajectory and velocity calculations. The bubble path is captured by overlapping field-of-views up to a height of 270 mm. Illumination of the region is provided by a white-backlight. Considering that typical lateral motion of an ellipsoidal bubble ($\approx$ 1.8 mm) is circa10 mm, which is much smaller than the column diameter (150 mm), any elongation effects in the bubble shape, due to refractive index associated with the column curvature, can be ignored. Acquired images are processed with open-source software FIJI (Schindelin et al., 2012) to obtain bubble characteristics, as described further.

2.3. Image analysis

A selected sequence of images is analyzed to obtain the bubble geometrical and motion parameters. The sequence of the image

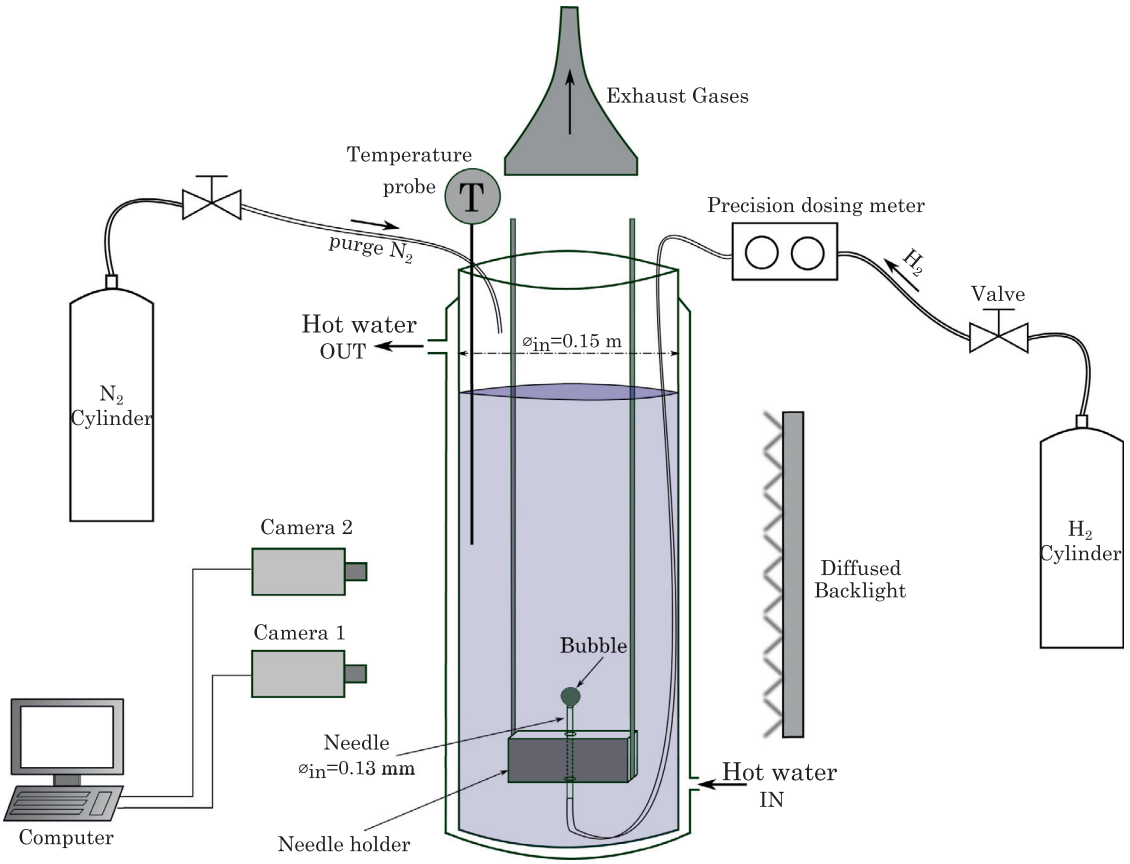

Fig. 2. A schematic of the experimental setup. Water flow in the jacketed part of the column is connected to a thermostatic water bath (not shown in the figure).

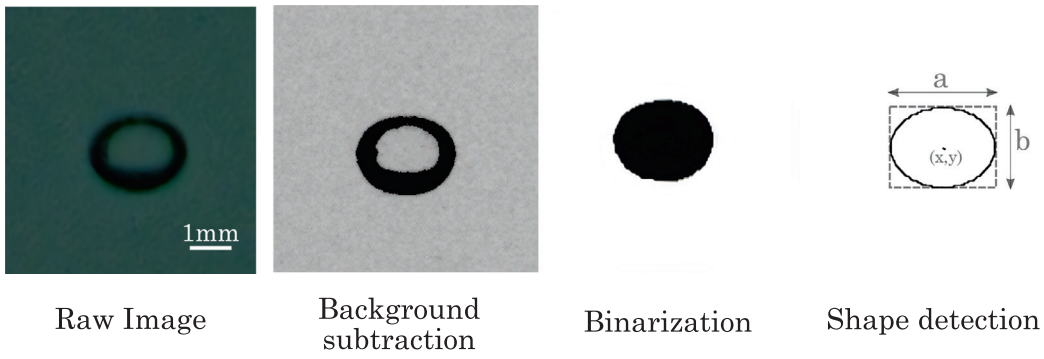

Fig. 3. Image processing steps in FIJI software.

processing steps is shown in Fig. 3. From raw images, the bubble outlines are generated using three steps: (i) background homogenization and subtraction, (ii) binarization, (iii) shape detection. The outlines are further analyzed to obtain, for each frame, the centroid coordinates (x,y), the horizontal and vertical lengths of the bubble, a and b, respectively. The bubble equivalent diameter, d_{eq}, is evaluated with an assumption of a spheroidal shape, with the vertical axis as the symmetry axis (Eq. (1)). The bubble aspect ratio χ is defined as the ratio of horizontal to vertical lengths of the bounding rectangle (Eq. (1)). The mean rise velocity is measured considering only the vertical displacement of the bubble between several frames.

$$\chi = a/b; \quad d_{eq} = \left(a^2 b\right)^{1/3} \tag{1}$$

3. Results and discussion

3.1. Bubble size and rise velocity

The nature of the gas sparging has a strong influence on the growth and rise of bubbles (Tomiyama et al., 2002). The bubbles generated here have a low initial distortion; the flow through the needle is controlled to ensure complete bubble growth before its release into the liquid.

The bubble equivalent diameter measured just before detachment at the needle, for all experimental cases, is as shown in Fig. 4a. For the water and the NaCl solution cases, there is a clear decrease in the bubble size with an increase in the temperature. For the electrolyte mixture cases, there does not exist a clear trend,

however, for 100% concentration there is a clear increase in the bubble size with an increase in the temperature. The bubble formation is a complex process, involving the initial expansion, with its base attached to the tip of the needle, followed by formation of a neck and the detachment of the bubble from the tip of the needle, until the breakage of the neck and release of the bubble into the liquid (e.g. Kulkarni and Joshi, 2005). The bubble size is associated with the interplay between the different forces acting on the bubble during the formation process. In a very slow quasi-steady process, assuming that the bubble size is determined mostly by its initial expansion when attached to the tip of the needle, the bubble size results from the competing buoyancy force ($F_b = \rho g \pi d_{eq}^3/6$) and surface tension force ($F_\sigma = \pi d_N \sigma$), where d_{eq} is the equivalent diameter of the bubble and d_N is the internal diameter of the needle. An increase in temperature leads to a decrease in the surface tension and a relatively small decrease in the density of the liquid, i.e. leads to a decrease in σ/ρ. This explains (qualitatively) the decrease in the bubble size with an increase in the temperature, observed in the water and NaCl solution cases; it also indicates that for the electrolyte mixture cases there are other (more complex) mechanisms and forces which play a significant role in determining the bubble size. Note that the liquid viscosity has a relatively large change with the temperature and the formation and breakage of the neck could also be influenced by the effect of the electrolytes on the interfacial

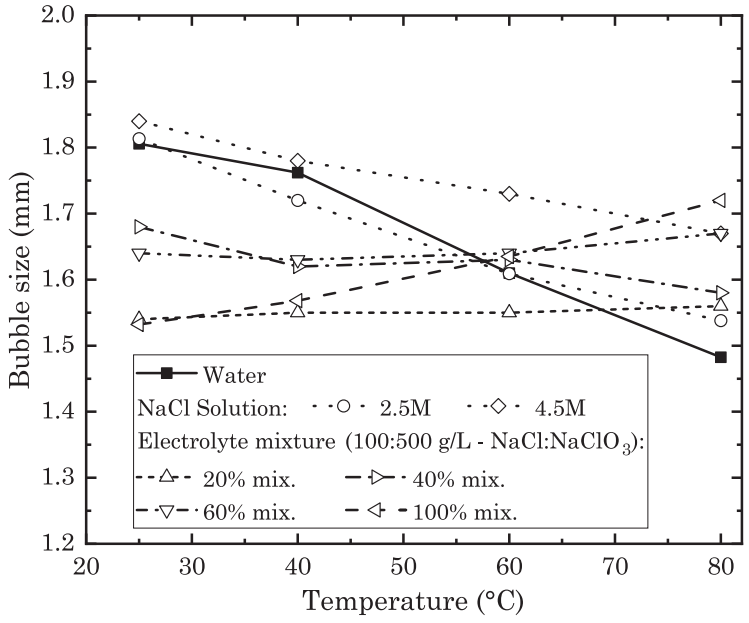

(a)

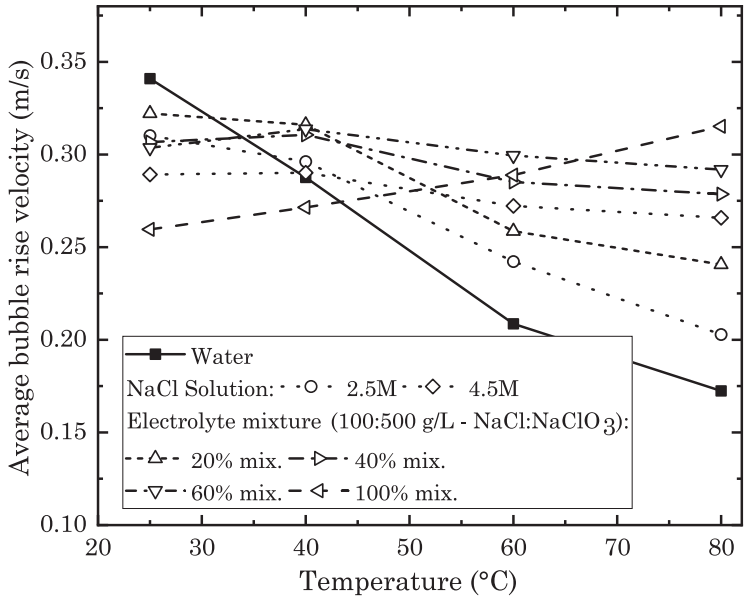

(b)

Fig. 4. Effect of electrolyte addition and temperature on: (a) average bubble size (equivalent diameter) at the needle, (b) average bubble rise velocity. Obtained from 5 measurements, with a standard deviation of 2.5% and 5.7%, respectively, for bubble size and rise velocity.

rheology (Appendix B), however, this is beyond the scope of this work, which is focused on the average terminal rise velocity of the bubbles.

The average terminal rise velocity (Fig. 4b), in general, decreases with an increase in the temperature, except for the electrolyte mixture with the highest concentration. While the initial bubble size and changes in fluid composition or temperature have been known to influence the rise velocity in the ellipsoidal bubble regime (1.5 mm $\leqslant d_{eq} \leqslant$4 mm) (e.g. Kulkarni and Joshi, 2005), the interplay between the different forces involved needs to be considered. For a better understanding of the relative effect of these forces and its effect on the bubble rise velocity, a non-dimensional analysis is required.

3.2. Non-dimensional analysis

3.2.1. Comparison with Clift Map

The four forces acting on the bubble (viscous, inertial, surface tension, and buoyancy) can be described in terms of three independent non-dimensional numbers. Among the many numbers that can be formed, the most common ones used in bubble physics are the Reynolds (*Re*), Eötvös (*Eo*), Morton (*Mo*) and Weber (*We*) numbers. Several efforts have been made in literature studies to describe the bubble shape and rise velocity in terms of these numbers (e.g. Kulkarni and Joshi, 2005). A well-known example is the classical empirical regime map (between *Re, Eo, Mo*) generated from experimental data for clean bubbles in pure fluids by Clift et al. (1978). For a bubble of known size rising in a fluid with known physical properties (ρ, μ, σ), an empirical *Re* can be determined from the map. The empirical Reynolds number, Re_{emp}, is obtained from digitizing the *Eo-Re-Mo* data. The experimental Reynolds number, Re_{expt}, is calculated from the average terminal rise velocity (U_T) and the bubble size obtained at the needle (just before detachment). Fig. 5a, shows an overlay plot of both Reynolds number, in the relevant range of *Eo* and *Mo*. A quantitative comparison (Fig. 5b) gives a good agreement between them, with an average deviation of 6%. This indicates that the rise velocity of a bubble in strong electrolyte solutions at all temperatures can be obtained from the knowledge of the bubble size and the properties of the fluids.

3.2.2. Parameterization

A standard representation of the bubble motion in a liquid medium is based on the drag coefficient, C_D. When a terminal rise velocity is reached, there exists a balance between the buoyancy and drag forces, and the drag coefficient can be expressed as:

$$C_D = \frac{4 d_{eq} g}{3 U_T^2} = \frac{4}{3} \cdot \frac{MoRe^4}{We^3} \tag{2}$$

Usually, the bubble rise is separated into three regimes (Tomiyama et al., 2002): (i) viscous force dominated regime, with small spherical bubbles and $Re \lesssim 10^2$; (ii) surface tension force dominated regime, with intermediate size ellipsoidal bubbles and $10^2 \lesssim Re \lesssim 10^3$; (iii) inertial force dominanted regime, with large spherical cap bubbles and $Re \gtrsim 10^3$. For a clean bubble in a pure liquid, if the bubbles are spherical, C_D= f(*Re*), and when the bubbles are not spherical (χ>1), C_D= f(*Re*, χ) (e.g. Moore, 1965).

For spherical clean bubbles in a pure liquid, in the limit of very high *Re*, C_D= 48/*Re*, and, from Eq. (2), a correlation for the bubble motion can be derived as:

$$Re = 2.047 We^{3/5} Mo^{-1/5} \tag{3}$$

However, for spherical bubbles at low and intermediate values of *Re* ($Re \lesssim 10^3$), the theoretical expression of C_D= 48/*Re* is not valid and, also, intermediate and large bubble sizes are not spherical.

Rastello et al. (2011) studied rising bubbles in silicon oils (Mo $\in$ [10^{-9};10^{-1}]) and found a similar empirical correlation, with the exponent of *We* becoming 2/3 instead of 3/5:

$$Re = 2.05 We^{2/3} Mo^{-1/5} \tag{4}$$

This slight change in the exponent of *We* (2/3 $\sim$ 3/5) indicates a low *We* dependency, which can be attributed to small deformations. This empirical correlation is also shown to be applicable to literature data on ultra-pure water (Duineveld, 1995) for intermediate bubble size ($d_{eq} \in$ [0.5 mm;1.5 mm]). However, the agreement of experimental data with Eq. (4) is limited to $Re \lesssim 300$. The deviation has been attributed to the onset of larger bubble deformations at moderate *Re* and its influence on the drag force.

Current experimental data shows a good agreement with $Re \propto We^{2/3} Mo^{-1/5}$, as shown in Fig. 6, and it can be represented through the following empirical correlation:

$$Re = 2.77 We^{2/3} Mo^{-1/5} \tag{5}$$

The increase in the proportionality factor for a clean bubble (from 2.05 to 2.77) can be attributed to the effects of the bubble shape (discussed in Section 3.2.3) and *Re*-regime ($Re \mathcal{O}(10^2 - 10^3)$). At higher *Re*, there is an increase in the aspect ratio, which leads to a change in the flow around the bubble and to a change in the pressure distribution along the bubble surface, ultimately contributing to an increase in the drag coefficient.

It is important to note here that the *Re* correlation of Eq. (5) describes the entire set of current experiments ($10^{-13} \leqslant Mo \leqslant 6x10^{-9}$, 0.74 $\leqslant We \leqslant$2.94), thereby, strongly indicating the role of the liquid properties in uniformly describing the rise characteristics of a bubble in strong electrolytes at varied temperatures.

3.2.3. Bubble deformation

Bubble deformation has been well-studied in terms of Weber number (*We*). Studying bubble rising in ultra-pure water ($d_{eq} < 1.8mm$), Duineveld (1995) proposed a correlation for the bubble aspect ratio (χ):

$$\chi_w = \frac{1}{1 - \frac{9}{64} We} \tag{6}$$

For a variety of fluids, a description of the bubble deformation would require a second parameter to reflect the viscous effects, either *Re* or *Mo*. Legendre et al. (2012), studying viscous liquids ($Mo < 10^{-3}$), proposed a dependency, based on *Mo*, for pure fluids as:

$$\chi_{pure} = \frac{1}{\left(1 - \frac{9}{64} We (1 + 0.2 Mo^{1/10} We)^{-1}\right)} \tag{7}$$

The presence of contaminants introduces additional stresses on the interface. A resultant effect is the reduction of the bubble aspect ratio. Compiling an experimental dataset of freely rising bubbles in contaminated solutions (surfactants, liquid mixtures, etc.), Loth (2008) proposed an empirical correlation:

$$\chi_c = 1/(1 - 0.75 \tanh(0.11 We)) \tag{8}$$

In Fig. 7, experimentally obtained aspect ratio data (χ_{expt}) is compared with the empirical correlations for pure and contaminated liquids. For a given *We*, only a marginal variation in the range of χ is observed, as expected from a $Mo^{1/10}$ dependence in low-*Mo* fluids. The current data shows a reasonable agreement with the pure liquids; a majority of data points are within the bounds defined by the range of *Mo* (-13 < log *Mo* < −8.5). Whereas a strong reduction in aspect ratio is expected for a bubble rise in a contaminated solution, it is not observed in the current experiments with a strong concentration of electrolytes, at all temperatures. This might be due to a

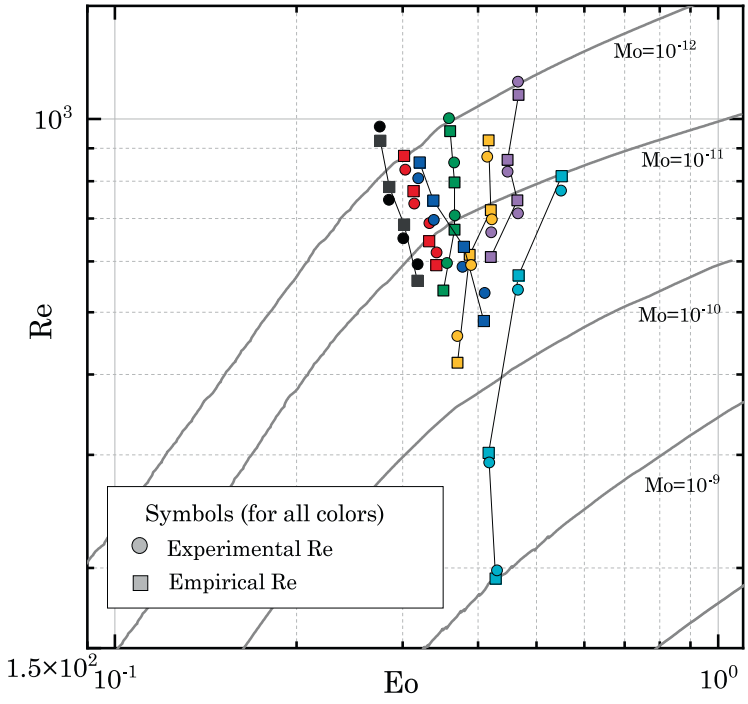

(a)

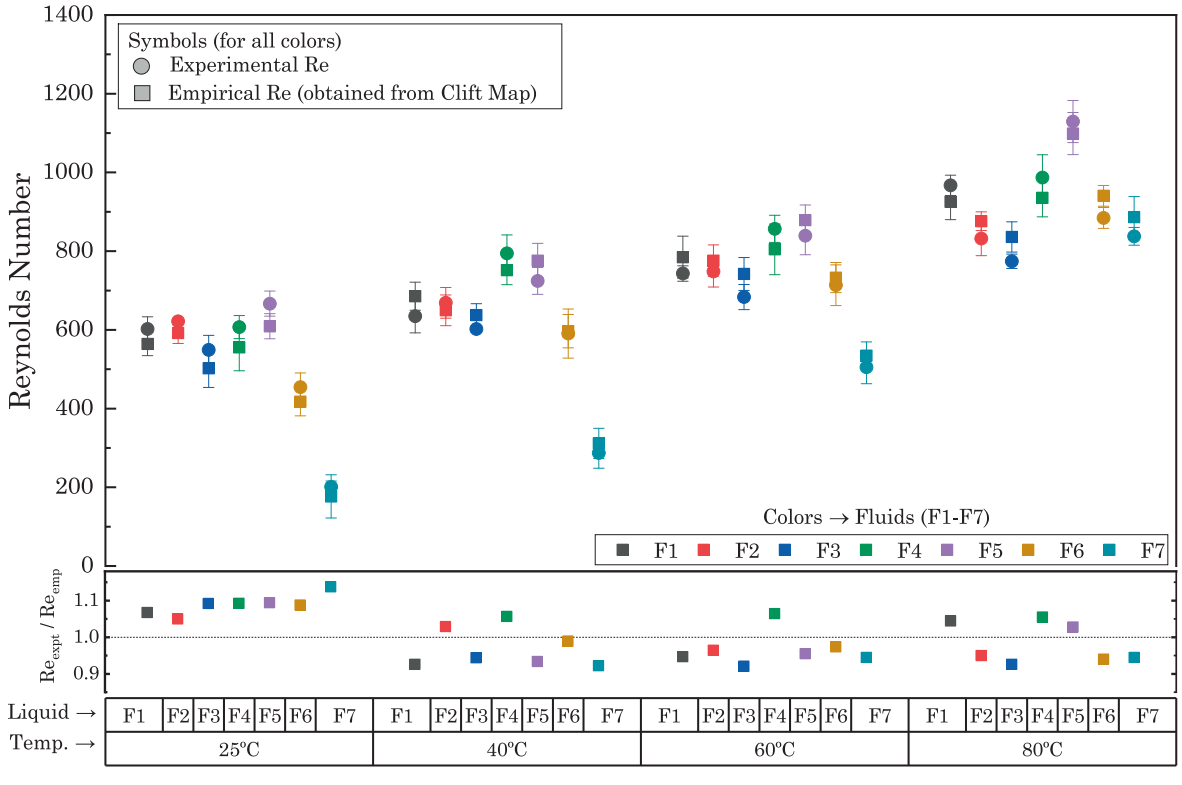

(b)

Fig. 5. (a) Clift map (Clift et al., 1978) (zoomed-in) with overlay data from current experiments. Markers denote Reynolds number, *Re* (○: experimental, Re_{expt}; □ : empirical, Re_{emp}); colours depict individual fluids F1-F7 (defined in A.1 in Appendix A). Four data points for each fluid indicates temperature; *Re* increases with increasing temperature. Lines are added for visualization purpose and do not indicate any correlation. (b) Reynolds number data for all experimental cases: a comparison between Re_{expt} and Re_{emp}.

lack of surface tension gradient along the bubble surface, as experimental studies on interfacial rheology (Safouane and Langevin, 2009; Hauner et al., 2017) show no dynamic behaviour at the interface due to presence of ions. We discuss this in Appendix B.

3.2.4. Drag coefficient

As mentioned earlier, the drag coefficient (C_D) is quite useful in understanding the bubble dynamics, especially for deforming bubbles. It is well-understood that shape effects and flow separation in

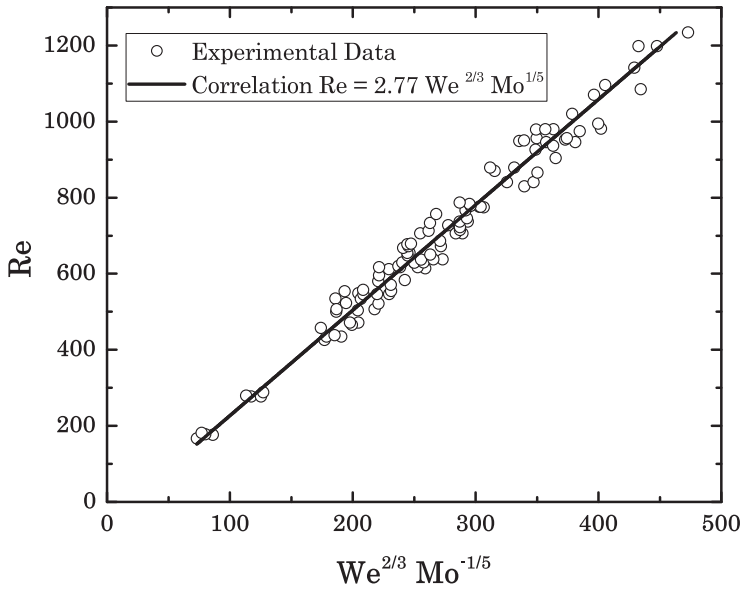

Fig. 6. Correlation betweeen *Re*, *We*, and *Mo* for all the experiments considered in this study. The solid line shows the correlation given by Eq. 5.

the bubble wake cause an increase in C_D, leading to a deviation from a universal dependence on *Re* (e.g. Moore, 1965; Loth, 2008). To describe C_D for a clean bubble in pure fluids, besides *Re*, another non-dimensional number would be required to take into account bubble deformation effects; most commonly used being *We* and *Mo*. While several empirical and theoretical correlations are available for the calculation of the drag coefficient (e.g. (Kulkarni and Joshi, 2005)), a majority of them are limited to lower *Re* ($Re < \mathcal{O}(10^2)$). A challenge being the accurate prediction of C_D in the ellipsoidal transition regime ($Re\ \mathcal{O}(10^2 - 10^3)$), relevant for the current work.

Rodrigue (2004) proposed an empirical correlation (Eq. (9)) of C_D=f(*Re*,*Mo*) that shows excellent agreement with experimental data (from Haberman and Morton (1953)) for a wide variety of pure liquids, for the entire range of *Re*.

$$C_{D,emp} = \frac{16}{Re} \times \frac{\left[1 + 0.020\left(\left[\frac{3}{4}C_{D,emp}Re^2Mo\right]^{8/9}\right)^{10/11}\right]^{10/11}}{\left[1 + 1.31\text{x}10^{-5}Mo^{11/20}\left(\left[\frac{3}{4}C_{D,emp}Re^2Mo\right]^{8/9}\right)^{73/33}\right]^{21/176}} \tag{9}$$

A comparison of current experimental data ($C_{D,expt}$, calculated from Eq. (2)) with predictions from Eq. (9) is presented in Fig. 8, showing a good agreement, with a deviation of 7%. This indicates that the drag force acting on the bubble can be expressed based on the properties of the fluids.

For a bubble rising in contaminanted liquids, the presence of even trace quantities of surface-active molecules or ions introduces a no-slip interfacial condition at the bubble surface. Whereas specific effects of contaminants at the interface are dependent on its nature and concentration, for practical purposes, an understanding is based on an incremental increase in drag (ΔC_D^*) due to the change in the interfacial condition and a decrease in the aspect ratio. Hence, the Weber number (*We*) becomes a relevant parameter. From an experimental dataset of contaminated fluids, Loth (2008) proposed a generalized equation for the drag coefficient $C_{D,c}$ (for 1<*We* <4) as:

$$C_{D,c}(We) = C_{D,We\to 0} + \Delta C_D^* \cdot (C_{D,We\to\infty} - C_{D,We\to 0}) \tag{10}$$

Here, $C_{D,We\to 0}$ represents the case of a rigid sphere and $C_{D,We\to\infty}$ represents the spherical cap case at highest deformation. The corresponding equations from literature (Schiller, 1933; Joseph, 2003) are:

$$C_{D,We\to 0} = \frac{24}{Re}\left[1 + 0.15Re^{0.687}\right]; C_{D,We\to\infty} = \frac{8}{3} + \frac{14.24}{Re} \tag{11}$$

As a function of *Re*, Eq. (10) establishes a link between the two regimes: spherical and spherical cap, to predict the values of intermediate *Re*, where the deformation has a strong influence on C_D. Recently, Rastello et al. (2017) showed that ΔC_D^* from Eq. (12) provided a good agreement with experimental data on tap water and contaminated silicon-oils, for *Re* < 700.

$$\Delta C_D^* = tanh(0.0055(WeRe^{0.2})^{1.6}) \tag{12}$$

$C_{D,c}$ for the current experimental range of 1<*We* <3 (gray region in Fig. 8) shows a clear dependence on *We* in the intermediate *Re* regime. However, the corresponding values for contaminated fluids are higher than the experimentally obtained C_D. Hence, the fluids used in the current study cannot be classified as contaminated.

A simpler drag coefficient equation can be obtained from the agreement of the experimental data with the empirical correlations (Eqns. 4 and 5), considering a generalized equation:

$$Re = XWe^{2/3}Mo^{-1/5} \tag{13}$$

where, *X* is 2.77 for the current data, in the intermediate *Re* regime, and 2.05 for the lower *Re* regime (Legendre et al., 2012; Rastello et al., 2011). In combination with Eq. (2), C_D = f(*Re*, *Mo*) can be expressed as:

$$C_D = \frac{4}{3}X^{9/2}Mo^{1/10}Re^{-1/2} \tag{14}$$

This equation is valid for a wide range of *Re* ($10^{-1} < Re < 10^3$) and for bubbles with limited deformation (1<We<4). At *We* ≫1, the drag coefficent tends towards a constant value, consistent with a spherical cap shape (Loth, 2008). For a pure fluid (given *Mo*), in the viscous dominated regime ($Re \lesssim 10^2$), Eq. (14) describes the departure from an uniform drag behaviour for a spherical bubble. With a dependence of $Mo^{1/10}$, for a higher value of *Mo* the departure

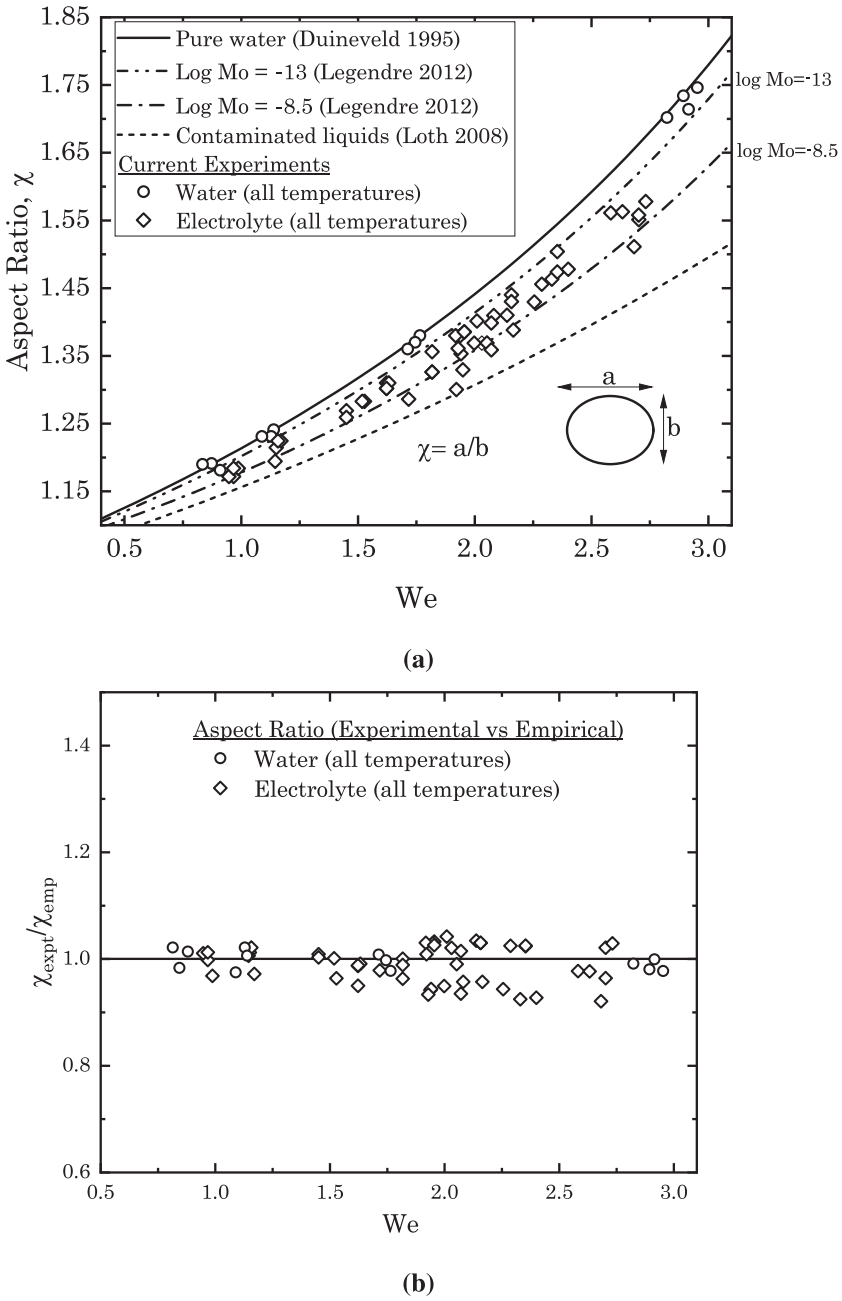

Fig. 7. Bubble aspect ratio (χ): (a) all experimental cases; (b) comparison with the empirical values, given by Eq. (6) (Duineveld, 1995) (for water cases) and Eq. (7) (Legendre et al., 2012) (for electrolyte cases).

occurs at a higher C_D and at a lower *Re*. In the intermediate *Re* regime, a higher value of the prefactor (X) accounts for an increase in the deformation effects on C_D. Here, X can be considered as a function of *We* and *Re*; in the limited range of *We*, X is dependent only on the *Re* regime. While derived from empirical correlations, from a practical perspective, a simple correlation (Eq. (14)) is useful in understanding the bubble behaviour for a variety of pure fluids, for $Re < 10^3$.

4. Conclusions

In the present study, the rise characteristics of a H_2 bubble at different temperatures, in water, NaCl solution, and various concentrations of a mixture electrolytes, has been studied. Our results strongly suggest that for high electrolyte concentrations, both collective and individual effects of the electrolyte concentration and temperature on the bubble rise velocity, the drag coefficient, and the bubble shape can be explained by their effect on the liquid properties (density, viscosity, and surface tension); experimental data agrees with known correlations for clean bubbles in pure liquids. Furthermore, similar to the existing knowledge on pure liquids, the bubble rise can be fully described non-dimensionally with the knowledge of the *Mo* and *We* numbers.

The current conclusions for high concentrations should not be extended to low concentrations (0.1–1 M); due to contradictory results (Quinn et al., 2014; Hessenkemper et al., 2020), it is not clear if the presence of electrolytes in this concentration range significantly affects the bubble rise velocity. At low concentration range, the change in the *static* surface tension and in the bulk properties of the liquid (viscosity and density) is relatively small, therefore, a significant effect on the rise characteristics of the bubble would have to be associated with the effects of the electrolytes

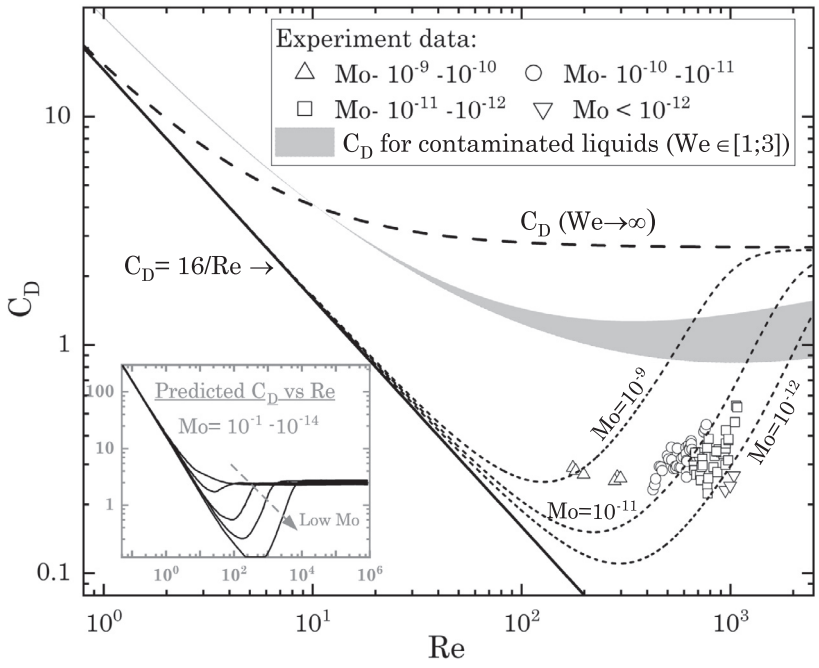

(a)

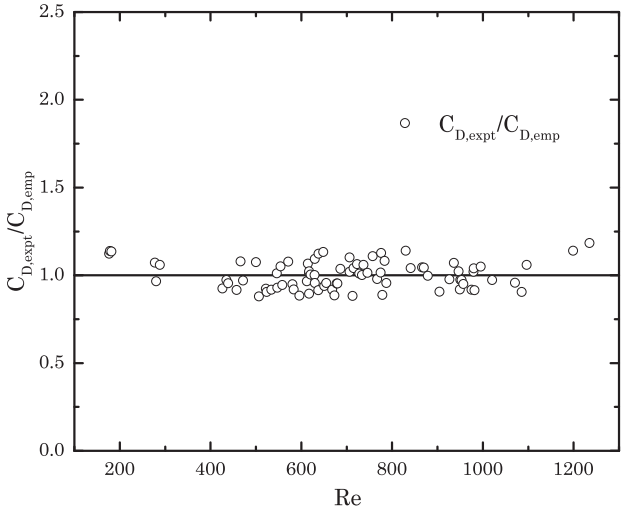

(b)

Fig. 8. (a) C_D vs *Re* plot: symbols indicate the experimental C_D; dashed lines (– – – – – –) are empirical prediction lines for Mo = 10^{-9}, 10^{-11} and 10^{-12}; gray zone depicts the prediction for contaminated liquids as f(*Re*, *We*); inset shows predicted behaviour for the entire range of *Re*. (b) Comparison of experimental C_D with the empirical values from Eq. (9) (Rodrigue, 2004).

on the interfacial rheology. These effects are dependent on the ion mobility and on interactions close the gas–liquid interface (detailed in Appendix B); a better understanding would be required to explain them and to clarify whether they can have a significant effect on the rise characteristics of the bubble. At higher concentrations, however, there is a relatively large change in the *static* surface tension and in the bulk properties of the liquid, which, just by itself, can change significantly the rise characteristics of an ellipsoidal bubble. This change in the properties (ρ, μ, and σ) is the dominant effect and the bubble rise can be explained by currently-known clean-bubble pure-fluid correlations based entirely on the *static* surface tension and in the bulk properties of the liquid (viscosity and density).

Declaration of Competing Interest

The authors declare that they have no known competing financial interests or personal relationships that could have appeared to influence the work reported in this paper.

Acknowledgements

This work is part of the grant Industrial Partnership Programme i36 *Dense Bubbly Flows* of the Netherlands Organization for Scientific Research (NWO), that is carried out under an agreement between Nouryon Industrial Chemicals B.V., DSM Innovation

Center B.V., SABIC Global Technologies B.V., Shell Global Solutions B.V., Tata Steel Nederland Technology B.V. and the NWO. The authors thank Bert Vreman for constructive discussions and comments on the manuscript. The authors also acknowledge additional financial support from the Nouryon PPC business unit and the industrial traineeship for MMM at Bohus, Sweden.

Appendix A. Properties of liquids

Table A.1

Appendix B. Ion effects and rheology of the gas–liquid interface

The presence of surface active ions/molecules at a gas–liquid interface can introduce additional rheological behaviour at the interface, affecting the interfacial tension gradient, and the viscous and elastic nature of the interface. The resultant effect on the interfacial rheology is dependent on the chemical nature and concentration of the species, their surface distribution and their transport kinetics between the interface and the bulk liquid. For the case of electrolytes, this appendix is intended to provide a literature understanding of the ion behaviour at the interface, its possible implications for the interfacial rheology, and, thereby, on the motion of a freely rising bubble. (Fig. B.1).

B.1. Interfacial ion mobility and static surface tension

The gas–liquid interface in pure water has a slight negative charge, as the OH^- ions are attracted to the surface, forming a dielectric layer (Chaplin, 2009). In electrolyte solutions, the behaviour of individual ions, including H^+ and OH^-, is dependent on its ionic size and charge. Electrostatic forces between the ions ultimately dictate the ion mobility and their distribution along the interface.

In an electrical double layer model, the distribution of charged species is known to occur within two layers close to the interface: ion-free layer and diffuse layer (Leroy et al., 2012). For the case of NaCl solution, both Na^+ and Cl^- ions would prefer to stay away from the interface; their interactions with H^+ and OH^- ions in the bulk are energetically more favorable (Jungwirth and Tobias, 2006). H^+ and OH^- are small ions and interfere with the transport process of other ions. Na^+ ions are small in size and hydrated by the water molecules surrounding it, as ion–dipole interaction is stronger than ion-ion one. Larger Cl^- ions are slightly polarizable and move towards the interface, however, face a strong repulsive force from the negatively charged interface, leading to an ion-free layer close to the interface. The potential at the interface, also called zeta potential, is dependent on the bulk ion concentration C_b. At bulk ion concentrations $C_b > \mathcal{O}(0.1M)$, increasing Na^+ ions can no longer be hydrated by H^+, leading them to move towards the interface. The net result is a reduction in the zeta potential (Yang et al., 2001).

The electrolyte ions are distributed in the diffuse layer, their interactions leads to a force imbalance between the bulk and the interface. A resultant change in the surface tension (σ) can be described, based on Gibbs adsorption isotherm, as:

$$d\sigma = -\Gamma_+ d\mu_+ - \Gamma_- d\mu_-; \Gamma_\pm = -\frac{1}{RT}\left(\frac{\partial\sigma}{\partial ln C_b}\right)_T \tag{B.1}$$

Here, $\mu_\pm$ (not to be confused with the liquid viscosity) are the chemical potentials of the cations and anions, and $\Gamma_\pm$ are the excess corresponding ions, per unit area of the interface, at a given temperature T. For both NaCl and $NaClO_3$, similar to most well-known electrolytes, there is an increase in the surface tension when compared to pure water; this increase varies linearly with the bulk

Table A.1
Physical properties of the liquids used in the current study.

Fluid (F#)	Temperature T, °C	Density ρ, kg/m^3	Viscosity μ, Pa.s, $\times 10^{-3}$	Surface Tension σ, mN/m	Morton No. $\mu^4 g/\rho\sigma^3$
F1	25	996	0.89	71.5	1.76×10^{-11}
Water	40	992	0.65	70.1	5.21×10^{-12}
	60	983	0.46	66.6	1.59×10^{-12}
	80	972	0.36	61.5	6.82×10^{-13}
F2	25	1085	1.13	75.9	3.48×10^{-11}
2 M NaCl	40	1076	0.83	73.7	1.08×10^{-11}
	60	1064	0.59	70.5	3.21×10^{-12}
	80	1053	0.45	66.5	1.36×10^{-12}
F3	25	1229	1.55	86.2	7.24×10^{-11}
4.5 M NaCl	40	1220	1.13	82.3	2.38×10^{-11}
	60	1209	0.81	77.2	7.55×10^{-12}
	80	1196	0.62	72.1	3.32×10^{-12}
F4	25	1091	1.21	85.0	3.17×10^{-11}
20% mix.	40	1082	0.91	81.2	1.16×10^{-11}
(0.94 M $NaClO_3$	60	1071	0.77	76.1	7.32×10^{-12}
+ 0.34 M NaCl)	80	1063	0.46	70.9	1.16×10^{-12}
F5	25	1157	1.36	87.2	4.44×10^{-11}
40% mix.	40	1148	1.09	83.3	2.08×10^{-11}
(1.88 M $NaClO_3$	60	1136	0.81	78.2	7.76×10^{-12}
+ 0.68 M NaCl)	80	1125	0.59	73.1	2.71×10^{-12}
F6	25	1192	1.56	92.1	6.32×10^{-11}
60% mix.	40	1166	1.21	87.4	2.69×10^{-11}
(2.81 M $NaClO_3$	60	1148	0.92	81.2	1.14×10^{-11}
+ 1.02 M NaCl)	80	1135	0.67	75.1	4.11×10^{-12}
F7	25	1367	3.46	101.1	1.01×10^{-9}
100% mix.	40	1358	2.27	94.3	2.28×10^{-10}
(4.69 M $NaClO_3$	60	1346	1.46	85.5	5.15×10^{-11}
+ 1.71 M NaCl)	80	1304	0.96	78.6	1.31×10^{-11}

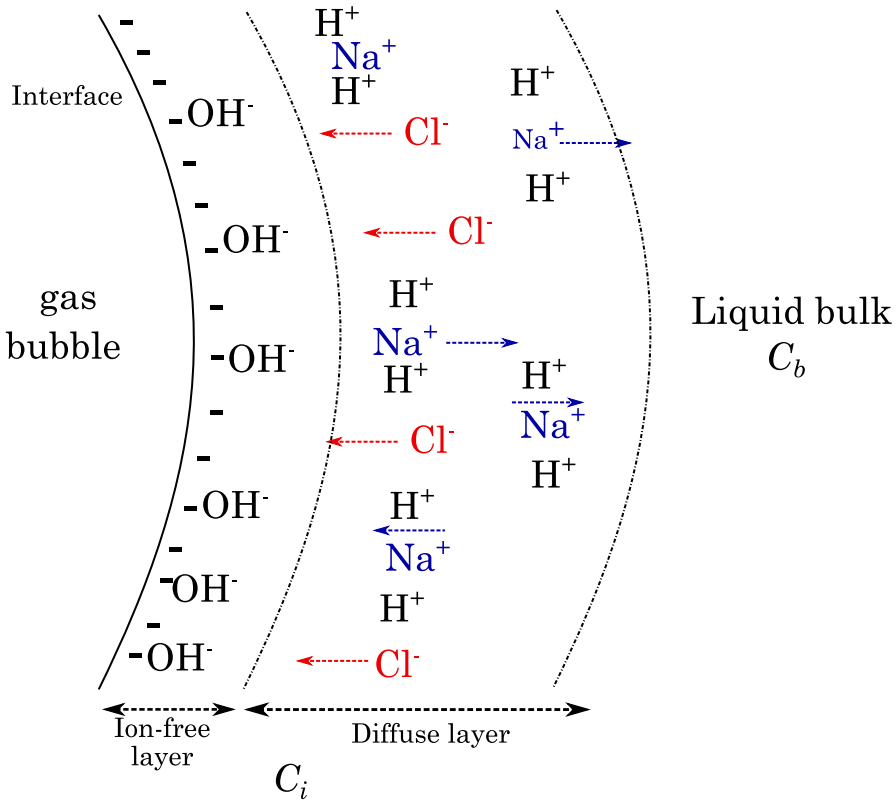

Fig. B.1. Schematic of ion distribution around gas–liquid interface in NaCl solution. Interfacial depths are in the range of 10–100 Å.

concentration (Henry et al., 2007). A higher $d\sigma/dc$ for NaCl (=1.76 mN m^{-1} M^{-1}), when compared to $NaClO_3$ (=0.72 mN m^{-1} M^{-1}), can be attributed to a higher polarizability of a larger chlorate ion, and as a consequence, a lower electrostatic repulsion. In the electrolyte mixture, besides the ion-specific effects, chloride-chlorate ion-interaction would also play a role in determining the net ion distribution at the interfacial sublayers.

B.2. Ion effects on interfacial rheology

A general understanding for all contaminants (salt, surfactants, mineral acids, etc.) is based on the Marangoni effect: due to non-uniform distribution of contaminants at the interface and adsorption/desorption transport processes occurring between the interface and bulk, the tangential stress along the bubble surface retards the bubble motion (Ruzicka, 2008). A possible consequence of contaminant addition is a change in the hydrodynamic boundary condition at the gas–liquid interface: from mobile to immobile. Depending on the contaminant concentration and bulk-interface transport kinetics, surface visco-elasticity and shear viscosity can be influenced (Langevin, 2014).

While Marangoni and other rheological effects are well-known for surfactant solutions, the same mechanism may not be applicable for electrolyte solutions. At low concentrations (up to 0.2 M), a change in hydrodynamic condition was not observed for smaller bubbles ($<$ 1 mm): the terminal rise velocity was found to be agree with the mobile case (Henry et al., 2008). Using surface visco-elasticity measurements, Safouane and Langevin (2009) ruled out a change in the slip-condition at the interface up to 5 M electrolyte concentration. Similarly, no influence on the dynamic surface tension of the gas–liquid interface was observed due to electrolyte addition up to 5.5 M concentration, according to (Hauner et al., 2017), who mention the rapid timescale of ion-mobility ($<$ 1 ms) as a possible explanation. Fast kinetics, indeed, minimizes the interfacial tension gradient along the gas–liquid interface (Edwards et al., 1991). These literature studies suggest that electrolytes have no significant influence on interfacial rheology.

It is important to note that other widely studied application cases with electrolytes draw a different conclusion. Increased surface viscosity and, thereby, reduced surface mobility at higher ion concentrations has been cited as a reason for: slow drainage of saline thin films and inhibition of bubble coalescence (Nguyen, 2017), and stabilization of surfactant-laden foam films due to electrolyte addition (e.g. Jarek et al., 2016; Xu et al., 2009). However, such a conclusion cannot be extrapolated for the case of a freely rising bubble, as confinement effects in thin films ($\mathcal{O}$(100 nm)) and the presence of surfactant molecules can have a strong influence on the electrolyte ion distribution and mobility.

While an increasing electrolyte addition has an impact on the ion interaction and mobility close to the interface, current literature suggests that this merely leads to an increase in the *static* interfacial tension and has no/limited influence on the dynamic rheological properties of the interface.

Appendix C. Surface tension measurement

While there are many ways to measure the surface tension measurement of liquids (e.g. bubble pressure method, Wilhelmy plate), at higher temperatures there are strong limitations to these traditional methods. As the liquid needs to be heated and maintained at a higher temperature, any gradient can strongly influence the accuracy. Hence, an imaging-based technique is used for the current study. In a pendant bubble method, as shown in Fig. C.1 (a), a hydrogen bubble is generated and stabilized at the tip of a J-shape needle (0.45 mm inner diameter), surrounded by the liquid of interest in an elongated cuvette (LxDxH = 10 mm x 100 mm x 50 mm). Bubble images are captured using a high-speed camera (Basler Aca-1920-150uc) attached with 75 mm macro-lens. The

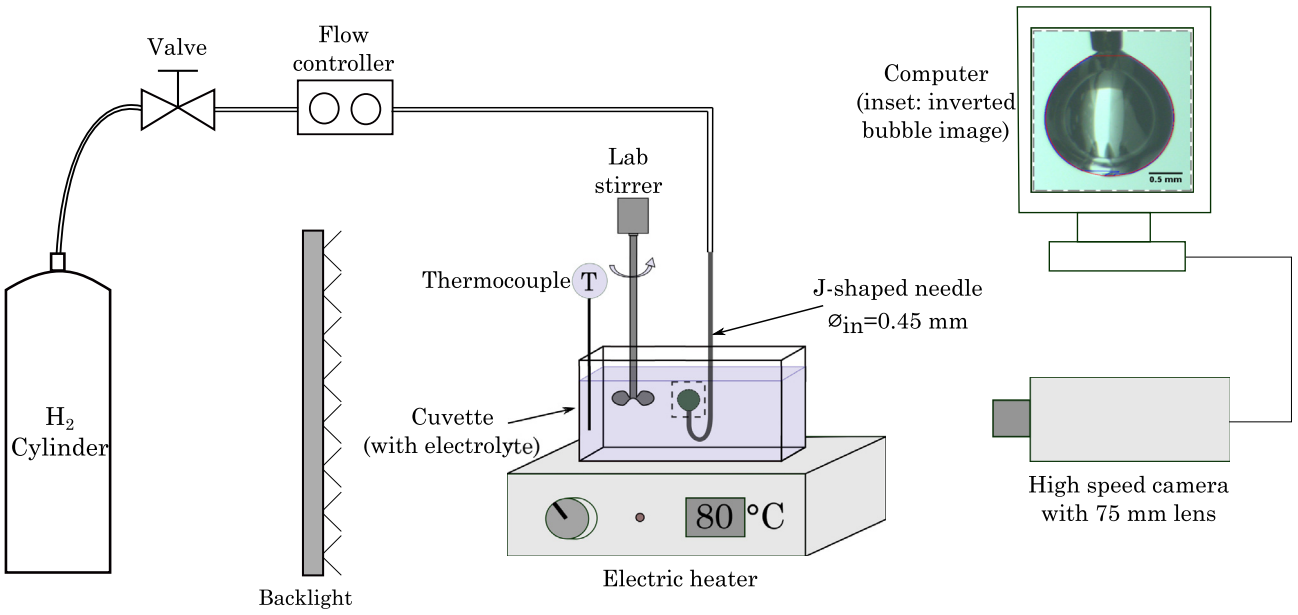

(a)

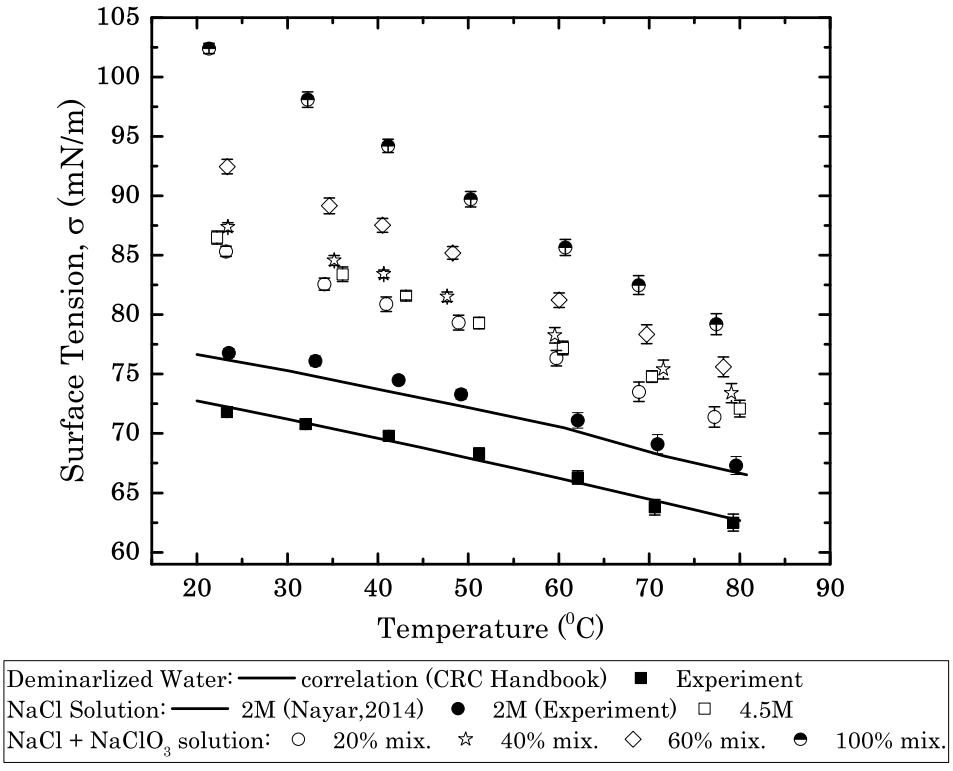

(b)

Fig. C.1. Measurement of liquid surface tension: (a) schematic of the setup with (inset) typical image of the bubble (inverted); (b) results for all liquids used in the current study.

bubble shape is the result reflective of the competing gravity and capillary forces. These images are inverted and subsequently analysed with Pendant drop analysis plugin (Daerr and Mogne, 2016), in FIJI software. Temperature is controlled using a laboratory electric heater. Temperature gradient is observed to be small ($\leqslant$0.5°C), as the cuvette is relatively small in size.

Results from the measurements (Fig. C.1(b) show an expected surface tension decrease with temperature and an increase with the addition of electrolyte. The imaging technique is quite reliable, with a maximum deviation of 0.5 mN/m, and the results for water and 2 M NaCl agree with known literature data (Haynes, 2009; Nayar et al., 2014).

References

Chaplin, M., 2009. Theory vs experiment: What is the surface charge of water? Water 1. doi:10.1.1.475.2221.

Clift, R., Grace, J., Weber, M., 1978. Bubbles, Drops and Particles. Academic Press, New York.

Cygan, R., 1991. The solubility of gases in NaCl brine and a critical evaluation of available data. Technical Report. Sandia National Laboratories Albuquerque (USA).

Daerr, A., Mogne, A., 2016. Pendent_drop: An ImageJ plugin to measure the surface tension from an image of a pendent drop. J. Open Res. Software 4. https://doi.org/10.5334/jors.97.

Duineveld, P.C., 1995. The rise velocity and shape of bubbles in pure water at high reynolds number. J. Fluid Mech. 292, 325–332. https://doi.org/10.1017/S0022112095001546.

Edwards, D.A., Brenner, H., Wasan, D.T., 1991. Interfacial Transport Processes and Rheology. Butterworth-Heinemann. https://doi.org/10.1016/B978-0-7506-9185-7.50013-1.

Fdhila, R.B., Duineveld, P.C., 1996. The effect of surfactant on the rise of a spherical bubble at high reynolds and peclet numbers. Phys. Fluids 8, 310–321. https://doi.org/10.1063/1.868787.

Haberman, W.L., Morton, R., 1953. An experimental investigation of the drag and shape of air bubbles rising in various liquids. Technical Report. David Taylor Model Basin Washington DC.

Hauner, I.M., Deblais, A., Beattie, J.K., Kellay, H., Bonn, D., 2017. The dynamic surface tension of water. J. Phys. Chem. Lett. 8, 1599–1603. https://doi.org/10.1021/acs.jpclett.7b00267.

Haynes, W.M., 2009. CRC handbook of chemistry and physics: a ready-reference book of chemical and physical data. CRC Press, Boca Raton.

Henry, C.L., Dalton, C.N., Scruton, L., Craig, V.S.J., 2007. Ion-specific coalescence of bubbles in mixed electrolyte solutions. J. Phys. Chem. C 111, 1015–1023. https://doi.org/10.1021/jp066400b.

Henry, C.L., Parkinson, L., Ralston, J.R., Craig, V.S.J., 2008. A mobile gas water interface in electrolyte solutions. J. Phys. Chem. C 112, 15094–15097. https://doi.org/10.1021/jp8067969.

Hessenkemper, H., Ziegenhein, T., Lucas, D., 2020. Contamination effects on the lift force of ellipsoidal air bubbles rising in saline water solutions. Chem. Eng. J. 386, 121589. https://doi.org/10.1016/j.cej.2019.04.169.

Jarek, E., Warszynski, P., Krzan, M., 2016. Influence of different electrolytes on bubble motion in ionic surfactants solutions. Colloids Surf., A 505, 171–178. https://doi.org/10.1016/j.colsurfa.2016.03.071.

Jean, D., Lee, D., 1999. Effects of salinity on expression dewatering of waste activated sludge. J. Colloid Interface Sci. 215, 443–445. https://doi.org/10.1006/jcis.1999.6272.

Joseph, D.D., 2003. Rise velocity of a spherical cap bubble. J. Fluid Mech. 488, 213. https://doi.org/10.1017/S0022112003004968.

Jungwirth, P., Tobias, D.J., 2006. Specific ion effects at the air/water interface. Chem. Rev. 106, 1259–1281. https://doi.org/10.1021/cr0403741.

Kang, I.S., Leal, L.G., 1988. The drag coefficient for a spherical bubble in a uniform streaming flow. Phys. Fluids 31, 233–237. https://doi.org/10.1063/1.866852.

Kracht, W., Finch, J., 2010. Effect of frother on initial bubble shape and velocity. Int. J. Miner. Process. 94, 115–120. https://doi.org/10.1016/j.minpro.2010.01.003.

Kulkarni, A.A., Joshi, J.B., 2005. Bubble formation and bubble rise velocity in gas-liquid systems: a review. Industr. Eng. Chem. Res. 44, 5873–5931. https://doi.org/10.1021/ie049131p.

Langevin, D., 2014. Rheology of adsorbed surfactant monolayers at fluid surfaces. Annu. Rev. Fluid Mech. 46, 47–65. https://doi.org/10.1146/annurev-fluid-010313-141403.

Legendre, D., Zenit, R., Velez-Cordero, J.R., 2012. On the deformation of gas bubbles in liquids. Phys. Fluids 24, 043303. https://doi.org/10.1063/1.4705527.

Leifer, I., Patro, R.K., Bowyer, P., 2000. A study on the temperature variation of rise velocity for large clean bubbles. J. Atmos. Ocean. Technol. 17, 1392–1402. https://doi.org/10.1175/1520-0426(2000)017<1392:ASOTTV>2.0.CO;2.

Leroy, P., Jougnot, D., Revil, A., Lassin, A., Azaroual, M., 2012. A double layer model of the gas bubble/water interface. J. Colloid Interface Sci. 388, 243–256. https://doi.org/10.1016/j.jcis.2012.07.029.

Levich, V., 1949. The motion of bubbles at high reynolds numbers. Zh. Eksp. Teor. Fiz 19, 436ff.

Liu, W., Moran, C., Vink, S., 2013. A review of the effect of water quality on flotation. Miner. Eng. 53, 91–100. https://doi.org/10.1016/j.mineng.2013.07.011.

Loth, E., 2008. Quasi-steady shape and drag of deformable bubbles and drops. Int. J. Multiph. Flow 34, 523–546. https://doi.org/10.1016/j.ijmultiphaseflow.2007.08.010.

Mei, R., Klausner, J.F., Lawrence, C.J., 1994. A note on the history force on a spherical bubble at finite reynolds number. Physics of fluids 6, 418–420. https://doi.org/10.1063/1.868039.

Moore, D., 1963. The boundary layer on a spherical gas bubble. J. Fluid Mech. 16, 161–176. https://doi.org/10.1017/S0022112063000665.

Moore, D.W., 1959. The rise of a gas bubble in a viscous liquid. J. Fluid Mech. 6, 113–130. https://doi.org/10.1017/S0022112059000520.

Moore, D.W., 1965. The velocity of rise of distorted gas bubbles in a liquid of small viscosity. J. Fluid Mech. 23, 749–766. https://doi.org/10.1017/S0022112065001660.

Nayar, K.G., Panchanathan, D., McKinley, G.H., Lienhard, J.H., 2014. Surface tension of seawater. J. Phys. Chem. Ref. Data 43, 043103. https://doi.org/10.1063/1.4899037.

Nguyen, P.T., 2017. Stability and coalescence of bubbles in salt solutions in a bubble column and thin liquid films. phdthesis. School of Chemical Engineering, The University of Queensland. doi:10.14264/uql.2017.445.

Okawa, T., Tanaka, T., Kataoka, I., Mori, M., 2003. Temperature effect on single bubble rise characteristics in stagnant distilled water. Int. J. Heat Mass Transf. 46, 903–913. https://doi.org/10.1016/S0017-9310(02)00345-9.

Peters, F., Els, C., 2012. An experimental study on slow and fast bubbles in tap water. Chem. Eng. Sci. 82, 194–199. https://doi.org/10.1016/j.ces.2012.06.061.

Quinn, J., Maldonado, M., Gomez, C., Finch, J., 2014. Experimental study on the shape-velocity relationship of an ellipsoidal bubble in inorganic salt solutions. Miner. Eng. 55, 5–10. https://doi.org/10.1016/j.mineng.2013.09.003.

Rastello, M., Marie, J.L., Lance, M., 2011. Drag and lift forces on clean spherical and ellipsoidal bubbles in a solid-body rotating flow. J. Fluid Mech. 682, 434–459. https://doi.org/10.1017/jfm.2011.240.

Rastello, M., Marié, J.L., Lance, M., 2017. Clean versus contaminated bubbles in a solid-body rotating flow. J. Fluid Mech. 831, 592–617. https://doi.org/10.1017/jfm.2017.624.

Rodrigue, D., 2004. A general correlation for the rise velocity of single gas bubbles. The Canadian Journal of Chemical Engineering 82. https://doi.org/10.1002/cjce.5450820219.

Rollbusch, P., Bothe, M., Becker, M., Ludwig, M., Grünewald, M., Schlüter, M., Franke, R., 2015. Bubble columns operated under industrially relevant conditions – current understanding of design parameters. Chem. Eng. Sci. 126, 660–678. https://doi.org/10.1016/j.ces.2014.11.061.

Ruzicka, M., 2008. On dimensionless numbers. Chem. Eng. Res. Des. 86, 835–868. https://doi.org/10.1016/j.cherd.2008.03.007.

Saad, S.M., Neumann, A.W., 2016. Axisymmetric drop shape analysis (ADSA): An outline. Adv. Colloid Interface Sci. 238, 62–87. https://doi.org/10.1016/j.cis.2016.11.001.

Safouane, M., Langevin, D., 2009. Surface viscoelasticity of concentrated salt solutions: Specific ion effects. ChemPhysChem 10, 222–225. https://doi.org/10.1002/cphc.200800527.

Schiller, L., 1933. Über die grundlegenden berechnungen bei der schwerkraftaufbereitung. Z. Vereines Deutscher Inge. 77, 318–321.

Schindelin, J., Arganda-Carreras, I., Frise, E., Kaynig, V., Longair, M., Pietzsch, T., Preibisch, S., Rueden, C., Saalfeld, S., Schmid, B., Tinevez, J.Y., White, D.J., Hartenstein, V., Eliceiri, K., Tomancak, P., Cardona, A., 2012. Fiji: an open-source platform for biological-image analysis. Nat. Methods 9, 676–682. https://doi.org/10.1038/nmeth.2019.

Sun, Q., Klaseboer, E., 2022. A universal model for drag on a spherical bubble. arXiv doi:10.48550/ARXIV.2204.03349.

Tomiyama, A., Celata, G., Hosokawa, S., Yoshida, S., 2002. Terminal velocity of single bubbles in surface tension force dominant regime. Int. J. Multiph. Flow 28, 1497–1519. https://doi.org/10.1016/S0301-9322(02)00032-0.

Tripathi, M.K., Sahu, K.C., Govindarajan, R., 2015. Dynamics of an initially spherical bubble rising in quiescent liquid. Nature Communications 6, 6268. https://doi.org/10.1038/ncomms7268.

Xu, Q., Nakajima, M., Ichikawa, S., Nakamura, N., Roy, P., Okadome, H., Shiina, T., 2009. Effects of surfactant and electrolyte concentrations on bubble formation and stabilization. J. Colloid Interface Sci. 332, 208–214. https://doi.org/10.1016/j.jcis.2008.12.044.

Yang, C., Dabros, T., Li, D., Czarnecki, J., Masliyah, J.H., 2001. Measurement of the zeta potential of gas bubbles in aqueous solutions by microelectrophoresis method. J. Colloid Interface Sci. 243, 128–135. https://doi.org/10.1006/jcis.2001.7842.

Zhang, Y., Sam, A., Finch, J., 2003. Temperature effect on single bubble velocity profile in water and surfactant solution. Colloids Surf., A 223, 45–54. https://doi.org/10.1016/S0927-7757(03)00189-4.